Journal of Sustainable Metallurgy (2024) 10:759–774
https://doi.org/10.1007/s40831-024-00825-2

RESEARCH ARTICLE

Effect of Particle Size and Starch Gelatinization on the Mechanical and Metallurgical Performance of Jarosite Plus Blast Furnace Sludge Self-Reducing Briquettes

G. Dall'Osto[1] · D. Mombelli[1] · V. Trombetta[1] · C. Mapelli[1]

Received: 20 October 2023 / Accepted: 2 April 2024 / Published online: 1 May 2024

Abstract

Jarosite and blast furnace sludge (BFS) are two of the main wastes from hydrometallurgical zinc production and iron production by blast furnace, respectively. Jarosite is a hazardous material that can, however, be reused in the steel industry after the recovering of the iron contained within it through carbothermal reduction in which BFS is exploited as a reducing agent. Yet, both wastes have a powdery nature that makes it necessary to agglomerate them for industrial use. On the other hand, despite the advantages of producing a self-reducing product, the particle size of the starting powders and the level of gelatinization of the binder could play a crucial role on the mechanical and metallurgical performance and, consequently, on the industrial applicability of the briquettes. Accordingly, two powder particle sizes (very fine sand vs. coarse silt) and three degree of corn starch binder retrogradation (10%, 30% and non-gelatinized starch) were used to produce briquettes, and their influence was studied by experimental and statistical investigation. The results showed that gelatinization plays the main role on the mechanical properties of briquettes, while particle size affects both density and reduction behavior; in particular, although all the mixtures were able to recover iron at 950 °C the most optimal mixture were obtained by using a granulometry of 63–125 µm for jarosite and less than 63 µm for BFS, while the local maximum of mechanical performance was obtained for a 30% starch retrogradation level.

Graphical Abstract

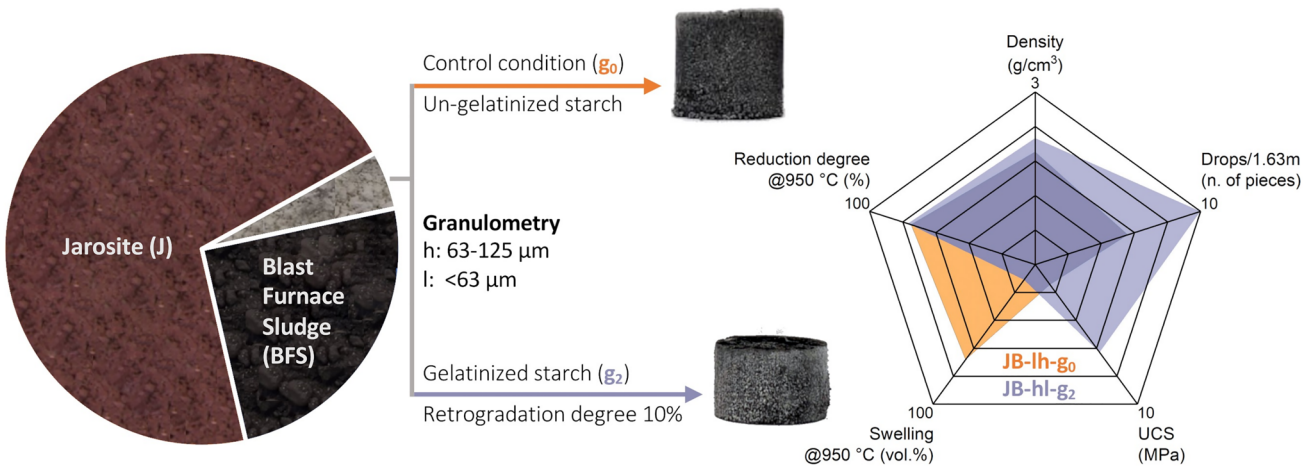

Keywords Jarosite · Blast furnace sludge · Self-reducing briquette · Starch gelatinization and retrogradation · Mechanical properties · Carbothermal reduction

The contributing editor for this article was M. Akbar Rhamdhani.

Extended author information available on the last page of the article

Introduction

Emphasizing the importance of recycling and valorization of industrial by-products or waste, precious metal recovery has become a crucial point for waste minimization and sustainable development [1, 2]. Among the wastes related to hydrometallurgical production of zinc, nickel, cobalt and copper, jarosite has attracted great interest, being an important iron oxide (40–50%wt.) and precious metals bearing material (e.g., Cd, Cu, Ni, Pb) [3, 4]. Consequently, the recovery of the nonferrous and ferrous fractions mainly, through hydrometallurgical and pyrometallurgical processes, is also very attractive in view of the fact that direct disposal of jarosite in landfills would create environmental problems due to the leaching of heavy metals, making it necessary to use stabilization processes such as Jarofix$^{(R)}$ [5–8].

Specifically, hydrometallurgy has found wide acceptance due to the possibility of selectively extracting the desired metal with a high yield, even from complex or impure feedstocks, which on the other hand can involve high costs due to the complexity of the process, the use of chemicals, and the subsequent maintenance of instrumentation to prevent corrosion [9]. Regarding the application of this process to jarosite, the recovery of nonferrous elements (e.g., Ag, In, Ni, Pb) has been studied in recent years with more than promising extraction yields (80–100%) [10–17]. Regarding the recovery of ferrous material from jarosite, pyrometallurgical processes have not yet been applied to their full potential, probably because of the need for intensive heat and the need of a reducing agent to achieve an optimal recovery rate, with even fewer studies focusing on Fe recovery conducted mainly in recent years and still characterized by a wide range of optimization [18–20].

Since industrial jarosite is usually in the form of dust ranging from clay to fine sand (less than 200 μm), if not properly managed the fine dust can be dispersed into the environment and cause health problems in addition to pollution [21]. Consequently, the exploitation of agglomeration techniques (e.g., briquetting and pelletizing), can overcome these problems and, more importantly, opens up the possibility of creating a solid product containing both the jarosite and the reducing agent necessary for metal recovery through pyrometallurgical processes [22, 23]. In addition, following a waste valorization perspective, every high carbon bearing material can be used as reducing agents.

In this regard, since 2019, Mombelli et al. [19, 24] investigated the exploitation of blast furnace sludges as a reducing agent, due to the high amount of C contained (~ 50%wt.), for iron recovery from different types of jarosite. The results showed that the chemical composition of the jarosite does not have a significant impact on the overall yield and the suitability of blast furnace sludge as reducing agent, with the highest iron oxide reduction always obtained for a C/Fe_2O_3 of 0.261. Accordingly, with the aim of creating self-reducing briquettes capable of valorize both jarosite and BFS, the role of the amount of binder (0, 5 and 10%wt.) and compressive pressure (20 and 40 MPa) on the performance of briquettes (⌀20 × 20 mm) was firstly studied in 2021, filling the gap present in literature regarding the making of such products [25].

Whilst the results of the 2021 study provided an initial know-how on the briquetting of jarosite and BFS, they were based only on the technological aspect and the process optimization has yet to be fully understood. Therefore, starting from the best briquetting parameters achieved (40 MPa and 5%wt. of corn starch as a binder), this study focuses on completing the process know-how by investigating the role of feedstock powder particle size (sand vs. silt) and the degree of retrogradation of corn starch, used as a binder taking inspiration from a 2^k factorial design [26]. The results of the mechanical (density variation over time, compressive and impact strength) and thermal (degree of reduction and swelling) experiments conducted on the different batches of self-reducing briquettes were used as the dataset to carry out the statistical analysis to show the main effect and interaction of granulometry and binder gelatinization time.

Materials and Methods

Raw Materials

The raw materials used for the briquettes production were jarosite (J), blast furnace sludges (BFS) and high purity quartz (> 95 wt.% SiO_2), used as a basicity corrector, which were chemically and mineralogically characterized in a previous work [24] through Energy Dispersive (ED-XRF) and Wavelength Dispersive X-ray Fluorescence (WD-RXF), total carbon and sulfur analysis, X-Ray Diffraction analysis (XRD) and Scanning Electron Microscopy with Energy Dispersive X-Ray Spectrometry (SEM–EDS); the main characterization results are provided in the supplementary material (Table S-I and Fig. S-1). Specifically, J was provided by a zinc smelter plant and were subjected to a drying process (105 °C for 24 h) and successive roasting treatment (1000 °C for 1 h) to remove the excess of water, obtaining a solid compound, and oxidize the most of sulfur present, respectively, by means of a muffle furnace. On the other hand, BFS were subjected to drying only.

Table 1 Jarosite-blast furnace sludges (BFS) pre-mixes labelling

		JAROSITE	
		< 63 µm	63–125 µm
BFS	< 63 µm	JB-ll	JB-hl
	63–125 µm	JB-lh	JB-hh

Table 2 Jarosite-blast furnace sludges (BFS) pre-mixes labelling

BFS respect to jarosite (wt./wt. %)	Quartz respect to jarosite (wt./wt. %)	C/Fe_2O_3	BI
35.93	16.35	0.261	0.504

Powder Briquetting

Roasted J and dried BFS were ground separately in a Retsch PM400 planetary ball milling machine (Retsch GmbH, Düsseldorf, Germany) with zirconium balls and namely sieved at very fine sand (h: 63–125 µm) and coarse silt (l: less than 63 µm) [26]. Malvern Morphologi 4 optical granulometer (Malvern Panalytical, Malvern, UK) was used to evaluate the particle size distribution of each powder according to the ASTM E2651-19 (2019) standard [27]. Four granulometric recipes (pre-mixes) were prepared by dry mixing J and BFS powders; the labelling of each recipe is reported in Table 1.

EMMA Mix Analyzer software (version 3.5.2.11, Elkem Materials Mixture Analyser) was used to predict the optimal packing of each pre-mix using the modified Andreassen model from the previously obtained particle size distributions. Based on literature considerations a distribution coefficient (q-value) equal to 0.28 and a particle size range of 0.2–180 µm were used to compute the target particle compaction curve [28].

Each pre-mix was based on a BFS/jarosite ratio of 0.36 ($C/Fe_2O_3 = 0.261$), and a binary basicity (BI) of 0.5, achieved by the quartz addition (sieved below 125 µm), to ensure the highest iron recovery in continuity with the previous works [24, 25]. The relative ratios between the feedstock powders are given in Table 2.

Corn starch was selected as organic binder and dosed to correspond to the 5%wt. of that of the specific pre-mix. Distilled water was added to the starch (starch-to-water ratio of 1:6 by weight) and the mixture heated at 80 °C for two dwell times (50 and 100 min) namely labelled g_1 and g_2. Furthermore, a control condition (g_0) was made just by the addition and mixing of starch and water without heating. The binder was immediately added to the pre-mixes and then pressed with a constant speed of 20 mm/min until 40 MPa and maintained for 2 min, using a modified uniaxial tensile test machine. Cylindric briquettes of 20 mm in diameter and 20 mm in height were produced and let dried for 14 days, during which the mass variation and visual appearance was monitored.

Corn Starch Retrogradation

The percentage of retrogradation (%R) of the g_1 and g_2 conditions was evaluated according to (1).

$$\%R = \frac{\Delta H_{retrogradation}}{\Delta H_{gelatinization}} \times 100 \quad (1)$$

The enthalpies were evaluated by means of differential scanning calorimetry using a DSC/823^e calorimeter (Mettler Toledo, Columbus, USA). For the retrogradation enthalpy 10 mg of g_1 and g_2 starch samples were taken and quenched in cold water (4 °C) before being hermetically sealed in a DSC pan, whereas for the gelatinization enthalpy 10 mg of g_0 starch was used; all the samples were subjected to a heating from 25 to 90 °C at a 10 °C/min scanning rate. The g_1 and g_2%R achieved namely corresponded to 30 and 10%.

Mechanical Characterization

The briquettes were mechanically characterized through cold compression and impact resistance test to simulate the real conditions at which they will be subjected during the industrial operations.

Cold compression test simulates the stresses at which the briquettes are subjected during the transportation or inside the furnace, the BS ISO 4700:2015 standard was used as a guideline [29]. The sample was pre-loaded between 2 flat plates at 30 N. The test started at a constant speed of 15 mm/min, and it was finished when the load falls by 50% of the recorded maximum value, or when the gap between the plates was reduced by more than 50% of the briquette diameter (10 mm). At the end of the test, the ultimate compressive strength (UCS) and energy absorption (EA) were determined.

Impact strength test simulates the fall of briquettes inside a furnace, the ASTM D440-07 (2019) standard was used as a guideline [30]. The sample were let fall from a of height of 1.63 m inside a tube with a vessel at the bottom to collect the sample after the crash to a maximum of 10 drops or until the fracture in several pieces. The material collected after the drops was sieved, and the weight fraction inside each sieve was weighted and evaluated as mass percentage with respect to the initial briquette mass. The sieves average opening sizes were 6.7 mm, 5.6 mm, 4 mm, 2 mm, 1 mm, 0.5 mm and 0.125 mm and they were normalized according to the biggest one for the size stability calculation, the size stability factor (s) of the briquettes was than calculated as visible in (2).

$$s = \sum_{\mathrm{i}} \%wt_i \cdot \frac{\text{Sieve Opening}_{\mathrm{i}}}{\text{Biggest Sieve Opening}} \tag{2}$$

The Impact Resistance Index (IRI) and the Adjusted Impact Resistance Index (AIRI) were calculated according to (3), (4) and (5). The former considers the ratio between the number of drops of each briquette and the number of pieces in which it breaks, whereas the latter also considers the powder detached during the drop test.

$$\text{IRI} = \frac{\text{Average Number of Drops}}{\text{Average Number of Pieces}} \times 100 \tag{3}$$

$$\text{Adjusting Factor} = 1 - \frac{\sum_i \frac{4}{S_i} \cdot M_i}{\text{Final Mass}} \tag{4}$$

$$\text{AIRI} = \text{IRI} \cdot \text{Adjusting Factor} \tag{5}$$

where S_i is the sieve opening (4 mm, 2 mm, 1 mm, 0.5 mm and 0.125 mm) and M_i the mass of powder detached from the briquette after the drop test and retained in the corresponding sieve. In this work, an arbitrary value of 4 mm (equal to half the briquette radius) was used as the maximum sieve opening. The product of the IRI value and the adjusting factor highlights how coarse is the powder lost during the drop test. The higher the difference between IRI and AIRI, the higher the amount of powder below 4 mm detached from the briquette and the worse the impact resistance of briquettes of equal IRI.

Metallurgical Performances Characterization

The briquettes were thermally treated at two temperatures (700 and 950 °C) to evaluate the swelling and reduction degree subsequent to the heating. The thermal cycles were carried in a Nabertherm LHT 02/17 LB lift-bottom furnace (Nabertherm, Lilienthal, Germany) in which a crucible containing the briquette was inserted. The crucible was made in alumina and to prevent any interaction with the briquette a second graphite crucible was used as briquette container. Since no variation of mass was observed in the graphite crucible along the experimental trials it was concluded that it did not affect the results. To ensure an inert atmosphere during the whole thermal cycle, an argon flow (10 Nl/h) was directly blown inside the alumina crucible to prevent any oxidation not related to the self-reducing briquettes themselves. After that the alumina crucible was saturated with argon, the samples were brought to the desired temperature with a heating rate of 100 °C/min, maintained for 30 min and then let cool to room temperature.

The swelling index was evaluated taking into account the apparent volume of the briquettes assuming the absence of internal porosities and according to (6).

$$\text{Swelling} = \frac{V_i - V_0}{V_0} \times 100 \tag{6}$$

where V_i is the briquette volume after the thermal cycle and V_0 is its initial volume. To obtain a clear estimation of the volume, the samples were digitally processed into 3D spatial data by means of Agisoft Metashape photogrammetric processing software (version 1.8.5, Agisoft LLC), both prior and after the thermal cycle.

The reduction degree (RD) was assessed using the BS ISO 11258:2015 standard as guideline and calculated according to (7) [31].

$$\text{RD} = \frac{w_i - w_0}{w_{th} - w_0} \times 100 \tag{7}$$

where w_i is the experimental mass of the sample after the thermal cycle, w_{th} is the theoretical residual mass after complete reduction and w_0 is the initial mass of the sample.

Mineralogical modification after the thermal cycles was determined by X-ray diffraction (XRD) analysis using a Rigaku Smartlab SE diffractometer (Rigaku Corporation, Tokyo, Japan) with CuKα radiation ($\lambda = 1.54$ Å) equipped with XRF suppression 1D detector (D/Tex 250). Manually homogenized powders through an agate mortar (below 100 µm) were scanned from 15 to 70° 2θ at 1°/min with a step size of 0.02° and rotated at 120 rpm to decrease texture contribution.

Design of Experiment

To statistically investigate the role of powder particle size (recipe granulometry) and binder gelatinization time on the briquette properties, the experimental campaign made use of two parallel 2^2 factorial design, the geometric representation of which is shown in Fig. 1.

Mechanical and metallurgical performance were set as the responses of the general linear model ANOVA, a probability value (p) less than 0.050 was considered statistically significant. The quality of the analysis and the validation of model assumptions (e.g., constant variance, independence of variables, and normality of the distribution) were assessed through observation of the residual plots. Finally, Bonferroni pairwise comparison was used to highlight differences in statistical significance among the four recipe granulometries [32]. The analyses were computed by means of Minitab software (version 21.4.1, Minitab LCC), and the results provided in the supplementary material.

Finally, the remaining gelatinization time (g_1) was used to create a new batch of briquettes, based on the most optimal

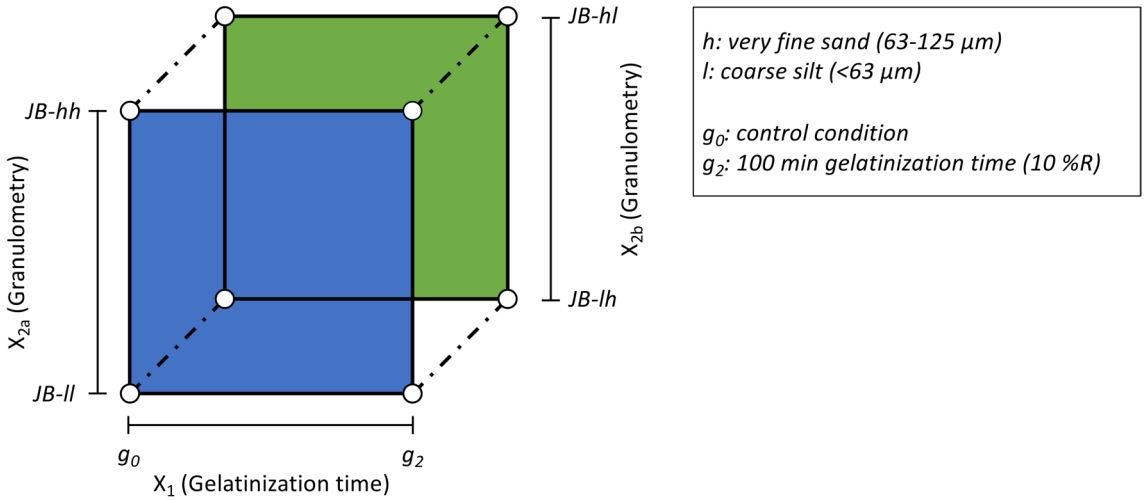

Fig. 1 Geometric representation of the proposed design of experiment

recipe, and compared with the respective previous results to complete the optimization of the jarosite-BFS agglomeration. A smelting process (1400 °C under Ar atmosphere) was carried out to evaluate the overall recovery of iron.

Results and Discussion

Powder Granulometry Characterization

The cumulative volumetric particle size distribution curves of J, BFS and quartz powder feedstocks and the particle compaction curves generated by EMMA are shown in Fig. 2.

The differences in the granulometric curve (Fig. 2a) was attributed to the mineralogy of the two feedstocks (e.g., higher presence of carbon in BFS and magnetite in J), which influenced their milling behavior, as well as the spontaneous agglomeration phenomena (e.g., presence of environmental moisture) that can take place during the sieving process [33]. More specifically, the particles obtained from the milling stage do not possess a perfectly round shape, but on the contrary, various broken surfaces and roughness, which inhibit sieving efficiency and results in the possible presence of particles with a larger diameter than expected in the granulometric curve, especially if elongated particles are present [34–36]. The presence of smaller diameter particles is due to the spontaneous re-agglomeration phenomenon due to ambient moisture related to the adhesion of smaller particles to larger ones, which once again reduces the separation efficiency of the sieving step. These agglomerates are then deagglomerated again revealing the presence of smaller diameter particle during the optical granulometry due to their spraying [33].

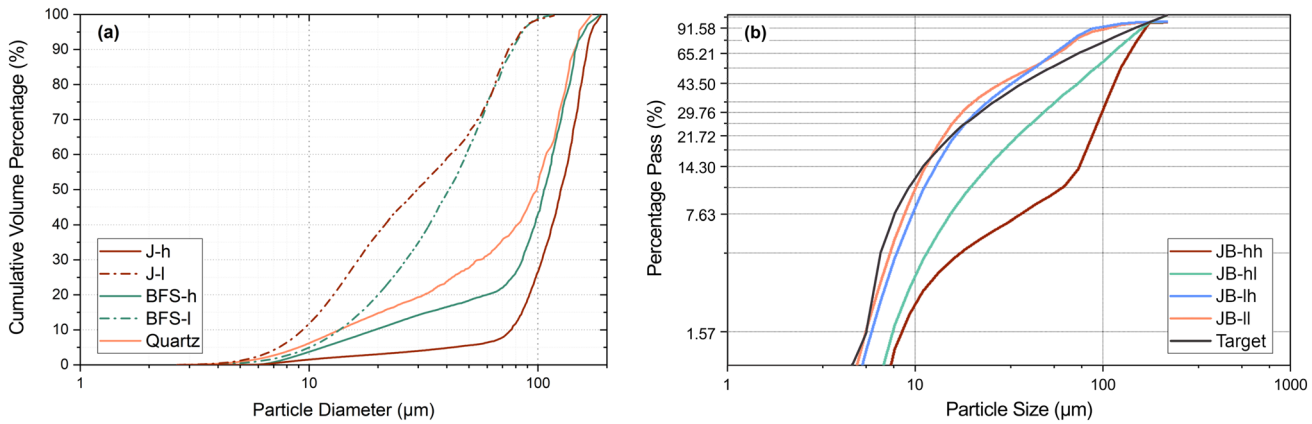

Fig. 2 **a** Cumulative volume percentage curve of powder feedstocks, **b** particle compaction curves generated by EMMA software (h: 63–125 µm, l: less than 63 µm, target line computed through modified Andreassen method)

The BFS-h particle distribution highlighted a shift towards the finer distribution respect to the J-h one and a higher volumetric percentage of particles finer than 63 µm, namely 20% in the former and 5% in the latter. Being J the main component in volume of the recipes the compaction curves were more strongly influenced by its granulometry respect to that of BFS. Indeed, the low percentage of particles in the 40–100 µm range of the J-h powder led to the significative deviation of the JB-hh recipe compaction curve from the target one (Fig. 2b). On the contrary, although a lack of particles in the 6–100 µm range was still present in the JB-hl recipe compaction curve the use of BFS-l powders decreased the deviation from the target. Finally, being the J-l granulometry more shifted towards the lower particle diameters (70% of particles lower than 63 µm), both the JB-lh and JB-ll recipe compaction curves nearly overlapped the target one.

Briquettes Characterization

The as-produced wet briquettes (green) were let dry for 14 days at room temperature to allow the binder retrogradation. Figure 3 shows the appearance comparison of the JB-hh-g_0 and JB-ll-g_2, taken as most representative of the respective batch, after the curing.

Both g_0 and g_2 briquette batches presented a sufficient strength to self-sustain themselves after the curing period with the presence of transverse cracks associated to the generation of shear stress during the demolding step of cold briquetting, more present and severe in the g_0 batch [37]. Longitudinal cracks running along the entire height of the briquette were occasionally observed in the g_0 batch, especially in the JB-hh-g_0 sample and referred to a bad powder compaction (Fig. 2b). During the curing period the formation of whitish needles was observed along all the briquettes surface, more wooly in the g_0 batch and more spiky in the g_2 batch. This phenomenon was already observed in previous studies involving jarosite as feedstock and addressed to the thenardite (Na_2SO_4)

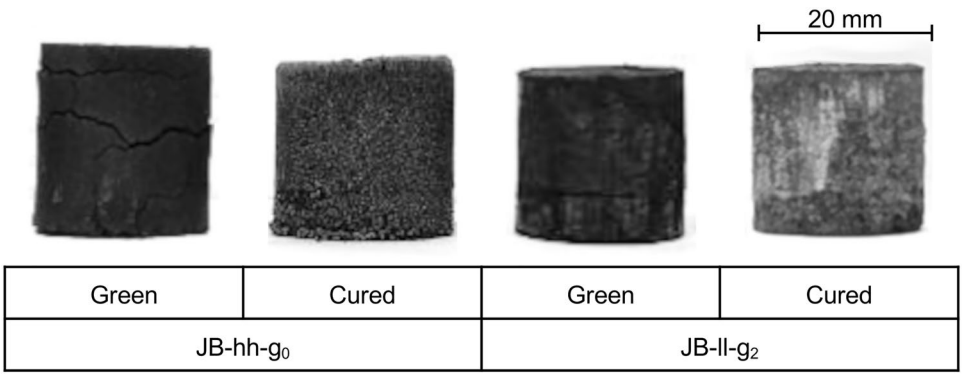

Fig. 3 Appearance of green and cured briquettes

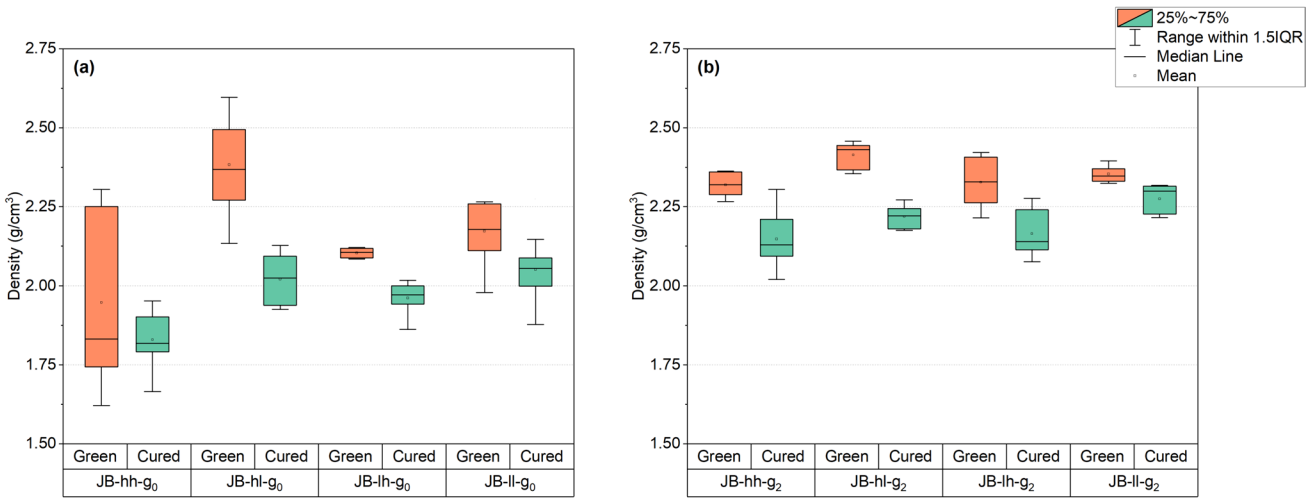

Fig. 4 Density of green and cured **a** g_0 batch briquettes and **b** g_1 batch briquettes

efflorescence [38–41]. The differences in the thenardite extent and appearance were related to the amount of water expelled from the binder network during its retrogradation, known as synesis, which are directly proportional [42]. Similarly, the overall higher decrease and scattering of densities observed for the g_0 batch was attributed to the absence of binder gelatinization (Fig. 4).

In both g_0 and g_2 batches the JB-hh recipe achieved the lowest density after curing, in accordance with what previously highlighted by the particle compaction curve (Fig. 2b) and what observed for biomass pellet production and curing [43, 44]. The higher densities achieved by the JB-hl recipe is attributable to the "loose particles" phenomenon according to which the briquetting process is able to generate a sufficient state of stress for the breaking of particles into finer granulometries, with a direct relationship between the volumetric fraction of particles generated and the initial granulometry [45]. Consequently, in the JB-hl recipe the loose particles generated by J are able to suppress the lack of fine particles previously highlighted by the JB-hl recipe compaction (Fig. 2b) enhancing its densification behavior. Since J is the main component in volume of the recipes it is assumable that the loose particle phenomenon is more evident when J-h powders are used rather than BFS-h, explaining the slightly lower mean density of the JB-lh recipe respect to that of JB-hl in both batches. Finally, the JB-ll recipes, and specifically the g_2 one which achieved the highest density, can be considered as a special case, since both the feedstock powders were sieved at the lowest granulometry and could hence considered as loose particles. The statistical analysis (Table S-II and Fig. S-2) highlighted the statistical significance of both the binder gelatinization and recipe granulometry as well as their interaction ($p < 0.05$). Furthermore, Bonferroni comparison confirmed the importance of the loose particle phenomenon, since the JB-hh recipe is the only one that shows a significant statistical difference when compared with the other recipes in the pairwise comparison (Fig. S-2b).

Cold Compression Test

The UCS and EA values obtained from the cold compression test are given in Fig. 5.

Direct comparison of briquettes from g_0 batch showed an increase in UCS and EA values coherent with the density of the corresponding recipe, the higher the density the higher the cold compression performances with the JB-ll-g_0 briquette achieving the highest UCS and EA (4.18 MPa and 0.22 mJ/mm^3), comparable to the respective g_2 batch recipe [45]. Although, the higher gelatinization time enhanced the mean UCS and EA values of all recipes (5.21–6.30 MPa and 0.29–0.50 mJ/mm^3 vs. 0.84–4.18 MPa and 0.22–0.03 mJ/mm^3 of g_2 and g_0 batches, respectively) the correlation between density and cold compression values seems to be less significant, all recipes having average values of 5.21–6.30 Mpa and 0.29–0.50 mJ/mm^3.

The experimental evidence of the greater influence of gelatinization over granulometry on cold compression values is also confirmed by the statistical analysis (Table S-III and Fig. S-3), according to which only the former has a statistical significance ($p < 0.05$), whereas granulometry as well as the interaction between the two factors results as non-significative ($p > 0.05$), Bonferroni comparison further confirmed the absence of statical differences between the recipes (Fig. S-3b).

The influence of binder can be explained by considering the failure mechanisms of the briquettes during the cold compression test. In g_0 batch, the network generated during the binder recrystallization is not sufficiently strong and diffused to provide an active contribution against the fracture propagation in the instability phase, localizing all stresses and cracks on the powders. On the contrary of g_2 batch

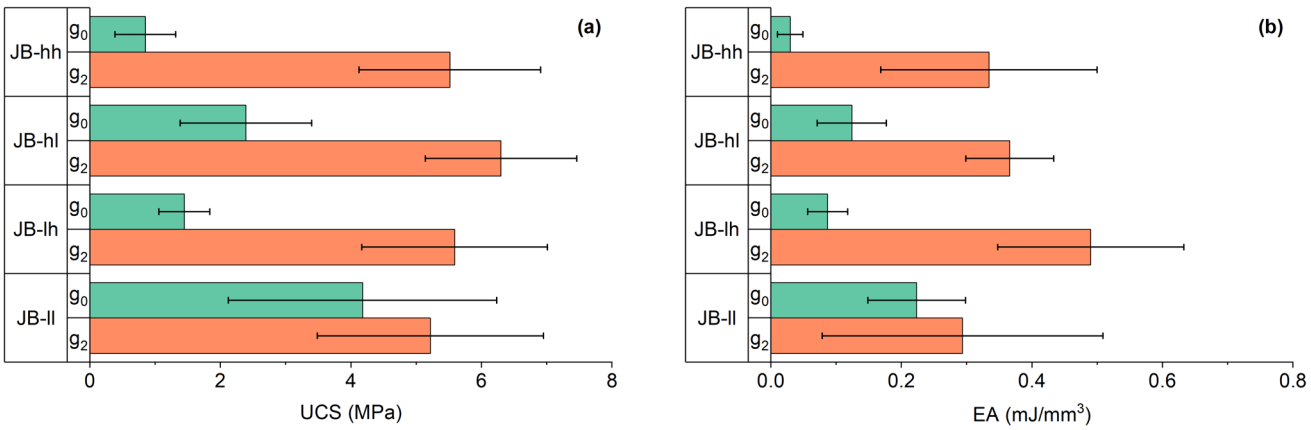

Fig. 5 g_0 and g_2 batches cold compression test results **a** UCS, **b** EA

network bond strength, which delayed the instability phase and the subsequent propagation up to rupture localizing the fracture initiation within the binder itself [46]. Furthermore, the influence of gelatinization was also evidenced by the appearance of the briquettes after compression: while the g_0 batch collapsed completely, the g_2 batch was able to keep the core of the briquettes intact, localizing the detachment of the material only on the outer surfaces. However, despite the acceptable performance of the g_2 briquettes, their UCS were lower than those obtained from similar studies using starch as binder (equal or higher than 12 MPa) [25, 47, 48]. A direct comparison between the values obtained by Mombelli et al. [25] and the JB-hh-g_2 briquette is of particular interest (12.42 MPa vs. 5.51 MPa). Specifically, an identical pre-mix was used, as well as the amount of binder added, but a shorter dwell time was used compared to g_2 (20 min. vs. 50 min.). This difference alone further reinforces the key role of binder gelatinization on the compressive strength of the briquette highlighted by the statistical analysis and suggests the presence of an optimal gelatinization value prior to g_2.

Drop Test

The results obtained from the drop test (IRI, AIRI and size stability) are reported in Fig. 6.

The gelatinization time of g_2 batch positively influenced both the IRI and AIRI indexes, independently by the recipe all the briquettes endured for 10 drops without breaking (IRI = 1000) against the average 2–3 drops of the g_0 batch briquettes. Furthermore, the lower difference between the AIRI and IRI indexes of the g_2 batch briquettes respect to that of g_0 ones, highlighted a considerably lower detachment of particles lower than 4 mm per drop. Similar to the cold compression, only the starch gelatinization resulted significative ($p < 0.05$), whereas the granulometry and the interactions between the two parameters is negligible ($p > 0.05$) (Table S-IV and Fig. S-4). Furthermore, Bonferroni comparison confirmed the absence of statical differences between the recipes (Fig. S-4b).

Finally, although the low number of drops sustained and low AIRI, the size stability of the g_0 batch briquettes were characterized by values between 90 and 100, highlighting a fines (< 125 µm) dispersion null or at least negligible. To investigate the causes of the poor performances of the g_0 batch, a failure analysis was carried out on the broken briquettes. The visual appearance of the JB-hh-g_0 briquettes, taken as most representative, and the SEM–EDS map of the fracture surface are given in Fig. 7.

In accordance with the highest state of stress, the crack propagated on a direction inclined at 45° respect to the base of the briquette, whereas the transverse cracks distributed along the outer surface have act as initiation point. The several white spots observed on the fracture surface were identified as thenardite due to the higher amount of Na and S observed respect to the matrix (Table 3). Since thenardite formation is associated with its efflorescence, its presence inside the matrix of the g_0 batch briquettes suggests that the removal of water occurring due to the synesis generated new surfaces (e.g., porosities) that were not filled by the network of bridges associated to the binder, thus allowing the thenardite crystallization [49].

Metallurgical Performance Characterization

Figure 8 shows the appearance of the briquette before and after the heating to 700 and 950 °C under Ar atmosphere; for each temperature and gelatinization level two briquettes per recipe are showed as main representative.

Both the g_0 and g_2 batch briquettes do not showed any significant visual appearance modification after the heating at 700 °C except for the removal of most of the thenardite previously present on the external surfaces.

Although its decomposition is expected at temperature higher than 700 °C, the presence of carbon or carbonate compounds decrease the decomposition temperature up to

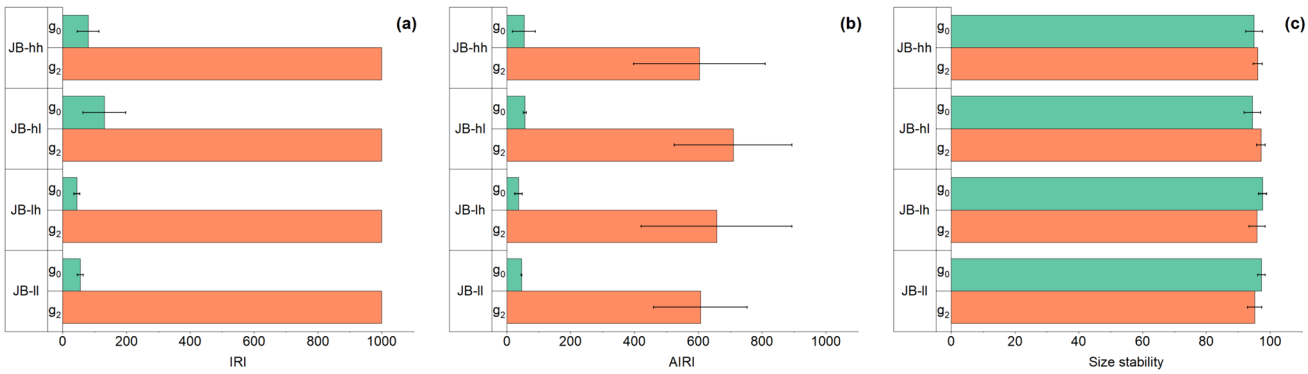

Fig. 6 g_0 and g_2 batches drop test results **a** IRI, **b** AIRI, **c** size stability

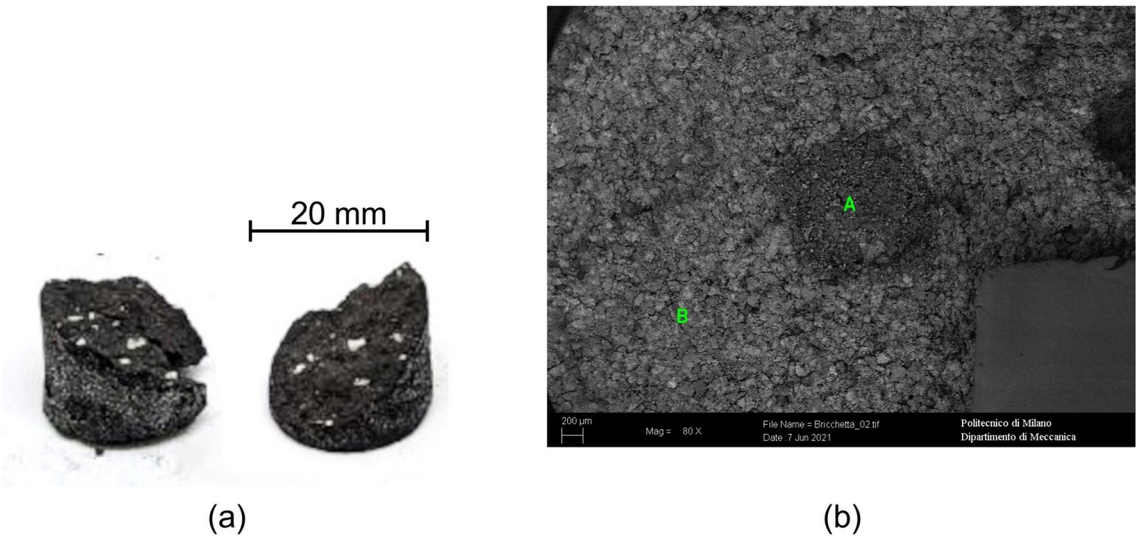

Fig. 7 JB-hh-g_0 briquette after drop test **a** visual appearance, **b** SEM micrograph of the fracture surface

Table 3 EDS spectra of JB-hh-g_0 briquette fracture surface (%wt.)

	C	O	Na	Si	S	Ca	Fe
Sp.A	37.18	42.39	3.68	3.38	5.11	4.88	3.38
Sp.B	57.19	25.40	2.47	4.04	1.34	2.56	6.99

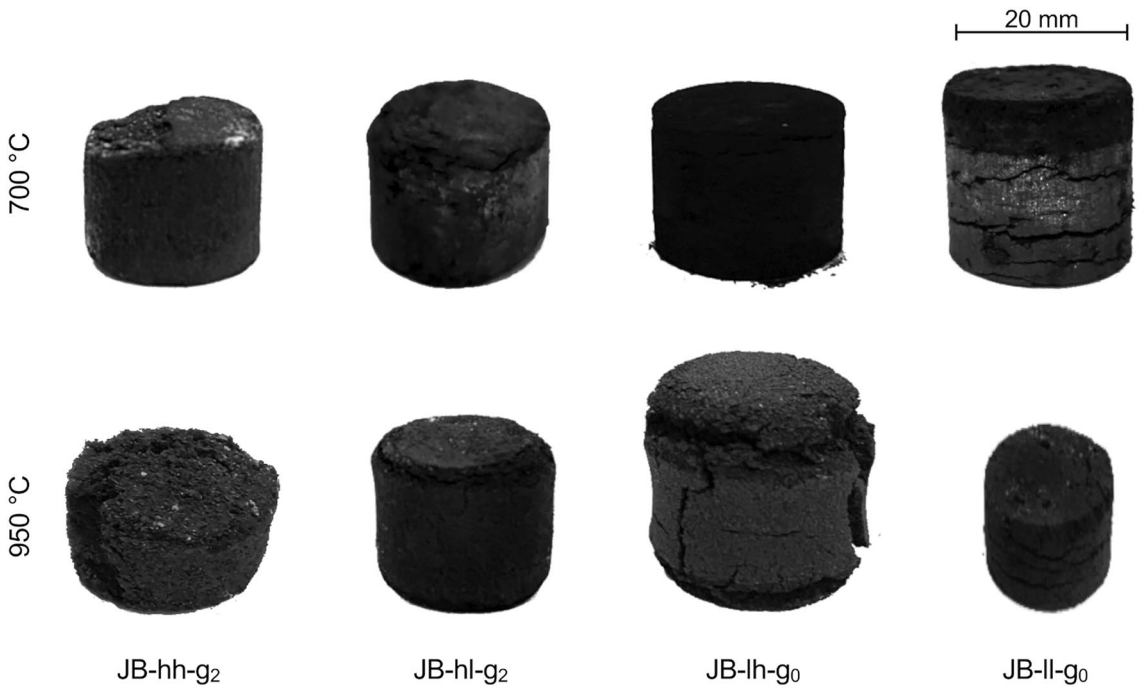

Fig. 8 Appearance of briquettes after heating at 700 and 950 °C

level close to the one used; whilst the use of an inert atmosphere is able to increase the decomposition rate [50–52]. For all the briquettes normal swelling (< 20%) was observed with a comparable RD ranging from 35 to 42% (Table 4), in agreement with the previous study on the metallurgical performances of J-BFS briquettes and other works regarding

Table 4 Metallurgical performances of g_0 and g_2 batches

		g_0				g_2			
		JB-hh	JB-hl	JB-lh	JB-ll	JB-hh	JB-hl	JB-lh	JB-ll
700 °C	Swelling (%)	6.54	10.83	15.27	13.45	7.65	10.58	5.25	5.39
	RD (%)	37.54	38.73	42.50	42.21	35.84	37.07	42.16	42.64
950 °C	Swelling (%)	76.64	68.22	67.94	-4.82	78.78	10.97	9.78	-9.75
	RD (%)	76.64	75.84	74.37	88.88	74.85	77.47	76.62	87.32

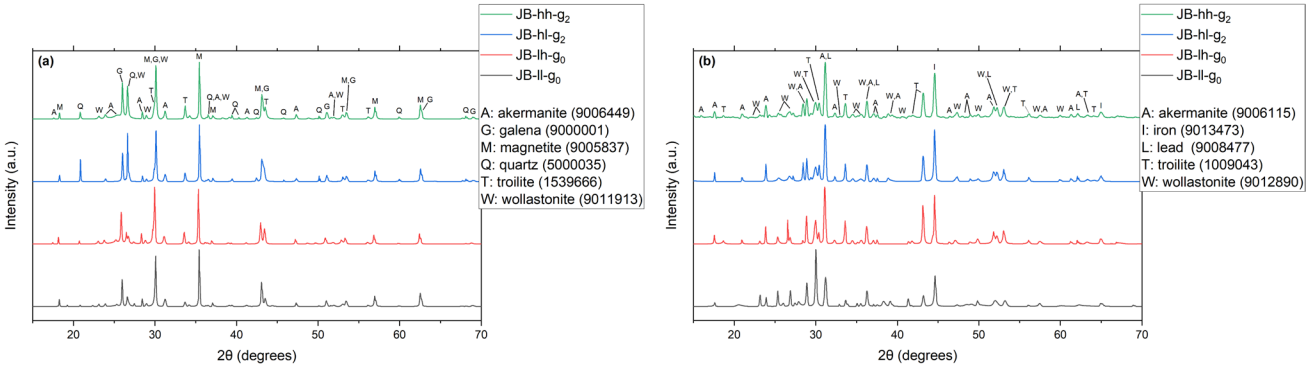

Fig. 9 XRD pattern of briquettes after heating at **a** 700 °C and **b** 950 °C

the reduction of iron oxide containing agglomerates heated at 700 °C [25, 53–55].

The slightly higher RD values of the JB-lh and JB-ll recipes of both batches were attributed to the higher surface-to-volume (S/V) ratio of the J-l particles, respect to the "h" granulometry, which enhanced the kinetics of the reduction reactions. The XRD patterns of the briquettes at 700 °C (Fig. 9a) highlighted the reduction of hematite (contained in the BFS powders) to magnetite as main phenomenon, whereas lead and iron(II) sulfides (galena and troilite) and calcium silicates (wollastonite) were already present in starting mineralogy of powders feedstock, with small differences in the peak intensity of the XRD pattern based on the recipe [24].

Significant visual appearance differences between the g_0 and g_2 batch briquettes were observed after the heating at 950 °C (Fig. 8b). On the one hand, the former were severely deformed due to the opening of the outer surfaces and the detachment of the upper and lower caps, with the only exception of the JB-ll-g_0 sample, which maintained its integrity; on the other the latter maintained a homogeneity upon heating without any severe alteration of their original shape. The different behavior, also reflected by the swelling index of the two batches at 950 °C (Table 4), was attributed to the presence of alkali and the role of binder network during the heating at temperature close to 1000 °C. According to literature the presence of alkali, even in low percentage, enhances the swelling of iron oxide containing agglomerates in the Boudouard reaction range (750–950 °C) and could lead to abnormal swelling with similar morphology of the one observed in this work [54, 56, 57]. Consequently, since the g_0 briquettes were characterized by the presence of thenardite inside their matrix, it is reasonable to assume that during the heating its decomposition locally increase the alkali concentration enhancing the swelling. The peculiar behavior of the JB-ll-g_0 briquette, as well as that of JB-ll-g_2, which were the only two briquettes characterized by a negative swelling (− 4.82% vs. − 9.85%), could be explained by considering the RD of all briquettes. Indeed, although the XRD patterns highlighted the complete reduction of magnetite into metallic iron for all the briquettes at 950 °C (Fig. 9b), JB-ll-g_0 and JB-ll-g_2 briquettes achieved a far superior RD (88.88% vs. 87.32%) respect to the average value of the others (74.37–79.85%) due to the higher reduction kinetics granted by the S/V ratio of the JB-ll recipe. Consequently, the phenomena occurring during the heating (e.g., compounds decomposition, gasification of carbon and formation of iron whiskers) as well as the sintering of the iron particles, which is considered to have a strong inhibiting towards the abnormal swelling, were anticipated [56]. On the contrary, the opposite occurred in the JB-hh-g_2 briquette, in which due to the lower kinetics induced by the high S/V ratio, the oxides reduction and iron sintering were delayed, hence leading to the lowest RD (74.85%) within the g_2 batch, and an abnormal swelling (78.78%). The role of S/V ratio was confirmed by statistical analysis (Table S-V and Fig. S-5), according to which recipe granulometry was the only significant parameter ($p < 0.05$). Furthermore,

Bonferroni test showed that the main significant difference was observed between JB-hh and JB-ll recipes, thus confirming the hypotheses made on the basis of experimental evidence (Fig. S-5b and Fig. S-5f).

On the contrary, although the statistical analysis showed the swelling behavior was not affected by both starch gelatinization and granulometry, as well as their interaction was not significant ($p > 0.05$), it is not possible to exclude that the normal swelling observed for the remaining briquettes of the g_2 batch is due to the active contribute of the starch network, which is expected to maintain the solid connection bridges up to 1000 °C, hence inhibiting the swelling [58]. Finally, Bonferroni comparison confirmed the absence of statical differences between the recipes (Fig. S-5d and Fig. S-5 h).

Briquette Performances Optimization and Binder Retrogradation Effect

The results from the statistical analysis revealed that corn starch gelatinization is the main parameter effecting the overall briquette performances, whereas the particle size of the feedstock modifies the results to a lesser extent, being it significative only on the briquette density and reduction degree (Table 5).

On this regard, the JB-hl recipe was chosen for the production of the third batch of briquettes (g_1). Furthermore, since the binder does not seem to have any statistical influence on metallurgical performance, the optimization of the briquettes focused solely on the mechanical properties at room temperature. However, it is conceivable, based on previous observations in this work, that an increase in mechanical properties is matched by an increase in metallurgical performance. Figure 10 shows the visual appearance and density of the green and cured briquettes of batch g_1, respectively.

Similar to the g_2 batch briquettes, the ones of the g_1 batch were only characterized by the presence of transverse cracks as well by the occurrence of thenardite efflorescence during curing (Fig. 10a). Specifically, due to the lower binder gelatinization the thenardite appeared slightly less crystallized respect to that of the g_2 batch. Moreover, although on the one hand the densities achieved by the g_1 batch were

Table 5 Summary of statistical significance of recipe granulometry and binder gelatinization with respect to mechanical and metallurgical performance of jarosite-blast furnace sludge briquettes

	Density	UCS	EA	IRI	AIRI	Size stability	RD (700, 950 °C)	Swelling (700, 950 °C)
Recipe granulometry	+s	−	−	−	−	−	+, +	−, −
Gelatinization	+s	+	+	+	+	−	−, −	−, −

+Significative, +s Significative with interaction, − Non significative

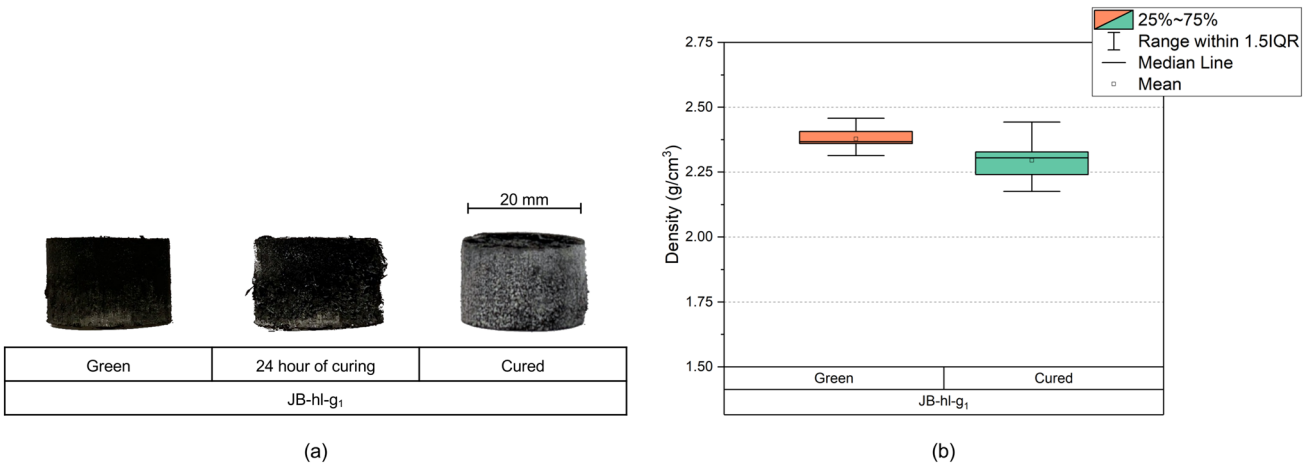

Fig. 10 JB-hl-g_1 green and cured briquettes **a** visual appearance and **b** respective density

Table 6 JB-hl-g_1 mechanical properties

	UCS	EA	IRI	AIRI	s
JB-hl-g_1	19.96 ± 2.93	1.34 ± 0.27	1000	792.79 ± 37.82	96.72 ± 2.15

comparable to the highest values previously obtained (Fig. 10b), on the other the mechanical performances were far superior (Table 6).

Specifically, the cold compression test highlighted an UCS and EA of 215% and 260% compared to that of JB-hl-g_2 briquette, whereas although the drop test results only achieved only a 10% increment of the indexes, the lower standard deviation of the AIRI index (37.82 vs. 184.12) pointed out a better homogeneity of the JB-hl-g_1 briquettes respect to JB-hl-g_2 ones and better performance compared to similar briquettes studied using starch as a binder [25, 47, 48].

The different behavior was attributed to the gelatinization and retrogradation processes of corn starch. Although the mechanisms are not completely understood, as depicted by several studies, during the heating once the amorphous fraction of starch (amylose) is completely destabilized, the crystalline phase (amylopectin) starts its gelatinization process, hence the higher the temperature and the dwell time, the higher the gelatinization degree [59, 60]. On the other hand, during retrogradation, the recrystallization of both the molecules takes place in a longer time span than gelatinization (minutes vs. days). Moreover, being gelatinization and retrogradation inversely proportional, and since in this study the binder was mixed with the feedstock powders prior to the initiation of the retrogradation, the experimental evidence highlights that the g_1 binder was able to better capture the feedstock powders within its gelatinized network respect to that of g_2 and g_0, confirming the statistical significance of the interaction between the binder and the recipe granulometry, previously observed [60]. Probably, during the curing period, in which retrogradation takes place, the final recrystallized network of the starch binder become denser, explaining the higher density achieved by the JB-hl-g_1 briquette, enhancing its mechanical performances [61].

Smelting Behavior and Iron Recovery

Following the main purpose of extractive metallurgy, consisting of the recovery of valuable metals from metal-containing ores or sources, and to close all the gaps on the know-how of jarosite and BFS briquettes, JB-hl-g_1 briquette was thermally treated at 1400 °C under Ar atmosphere for 30 min to evaluate its smelting behavior. The visual appearance of the briquette after smelting is shown in Fig. 11a. Compared with those treated at lower temperatures (Fig. 8) the JB-hl-g_1 briquette is characterized by an heterogeneous appearance due to the generation and subsequent solidification of a liquid slag during heating, and an overall shinier appearance, which can be associated with the presence of metallic iron droplets. In addition, while the melting process and intimate contact between the particles promoted briquette sintering, the latter hindered the mechanical separation of the recovered metal from the slag phase, which could be avoided by increasing the furnace residence time [62] or temperature [19]. Consequently, the samples were polished to expose the cross section, which was considered as most representative for evaluating the phase distribution and understanding the melting behavior (Fig. 11b).

The SEM observation of the cross section paired with the EDS spectra (Table 7) confirmed the presence of evenly

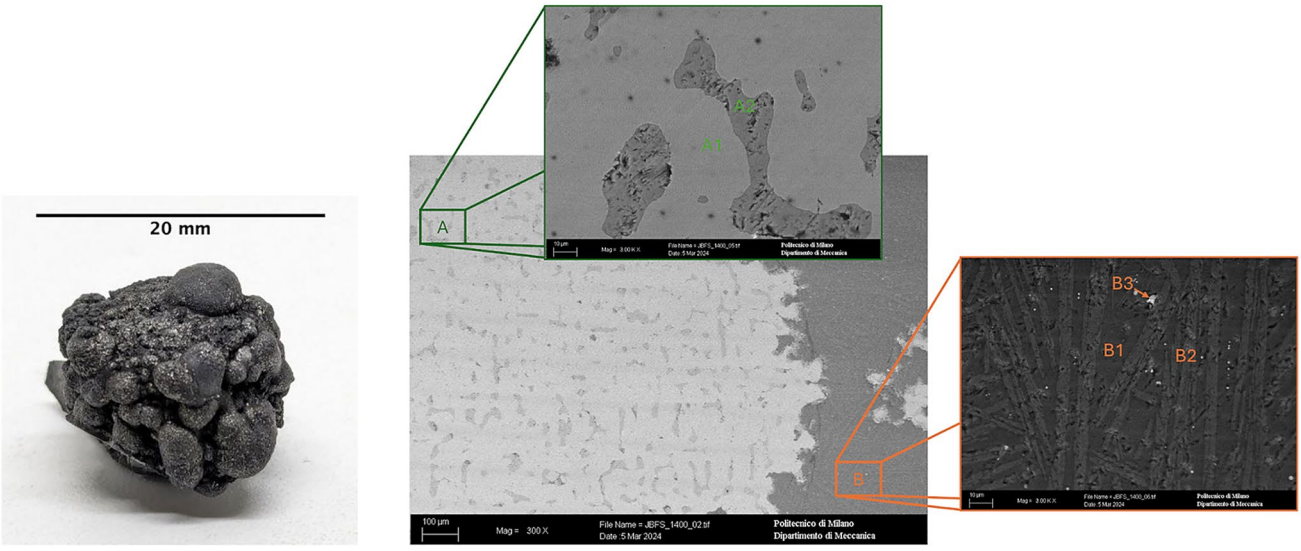

Fig. 11 JB-hl-g_1 briquette after smelting at 1400 °C **a** visual appearance and **b** SEM micrographs of the cross section with details at higher magnification of metallic matrix and slag

Table 7 EDS spectra of JB-hl-g_1 briquette (%wt.) and associated phase

	O	Na	Mg	Al	Si	S	Ca	Fe
Metal (area)					3.74	4.73		91.53
Sp.A1					4.64			95.36
Sp.A2						34.34		65.55
Slag (area)	35.95	2.81		3.09	30.85	6.59	17.83	1.25
Sp.B1	42.78				27.07	1.85	28.29	
Sp.B2	41.91	6.05	1.83	5.88	34.21		4.95	
Sp.B3	25.44				14.84	17.83	17.9	23.99

distributed islands of recovered metal throughout the surface and strongly linked to the slag phase.

Specifically, the areal EDS spectrum of the recovered metal was characterized by Fe as main element (91.53%wt.) and S (4.73%wt.). The point EDS spectra enabled the identification of two phases, the metal matrix, consisting of the recovered iron (Sp.A1 in Table 7), and the iron sulfides (Sp.A2 in Table 7), formed as a result of the sulfidation reactions (Reaction (8)). As observed in the previous work [24] concerning the description of the reduction behavior of BFS and jarosite used in this work and as described by Han et al. [63], in the 120–1200 °C range, volatile sulfur is easily captured by iron oxides in the matrix, while carbon acts as a promoter of sulfidation (8).

$$Fe_2O_3 + 2SO_2 + 7C \rightarrow 2FeS + 7CO \quad \Delta G = -1.0415T_{(K)} + 489.81 \tag{8}$$

The slag phase was characterized by a calcium silicate matrix, within which sulfur was dissolved (Sp.B1 in Table 7), and elongated andesine ($(Na,Ca)(Si,Al)_4O_8$) crystals nucleated and grown (Sp.B2 in Table 7). In addition, the presence of small iron sulfide particles dispersed in the slag phase (Sp. B3 in Table 7) was evidenced, similar to what was previously observed during the cast iron production through the jarosite reduction via arc transferred plasma reactor [20].

Finally, since SEM characterization did not reveal the presence of residual iron oxides either in the slag or in the metal phase, the total conversion of iron oxides (reduced and sulfidated) is equal to 100%, while the degree of metallization must be expressed as a function of the recovered metallic iron relative to the total observed iron content (iron as metal plus iron as sulfide), resulting in 89.47%.

Consequently, for practical application of the recovered iron, strong desulfurization is required, which can be achieved either by increasing the basicity of the pre-mix [19] or by using a desulfurizing slag after iron tapping/recasting [64].

Conclusion

With the aim of achieving a deeper know-how of the briquetting process of jarosite and blast furnace sludges by means of corn starch, this work took advantage of statistical analysis and experimental observations to investigate the role of the feedstock powders granulometry and binder gelatinization on the mechanical and metallurgical performances of such briquettes. The main conclusions of the current study can be summarized as follows:

- Statistical analysis showed that the mechanical properties of briquettes are mainly influenced by starch gelatinization. In contrast, feedstock powder granulometry and its interaction with gelatinization, albeit significant for the briquettes' density, can be exploited to fine-tune their performance at room temperature.
- At the same time, although only the powder particle size has a small influence on the reduction degree, experimental evidence has led to the hypothesis that the binder network plays a key role in counteracting swelling. Which can be further inhibited through the increase of fine particles in the starting mixture due to the increased kinetics of the reduction reaction, thus anticipating the sintering of the briquettes.
- Starting from the best recipe granulometry (JB-hl), the mechanical properties were significantly improved by decreasing the gelatinization time of the binder, and consequently increasing the degree of retrogradation from 10 to 30%, highlighting the presence of a local maximum of mechanical performance and the possibility of further studying the most optimal degree of retrogradation of gelatinized corn starch for the production of jarosite and blast furnace sludges self-reducing briquettes.
- The presence of two competitive reactions (iron oxide reduction and sulfidation) lead to a final degree of metallization equal to 89.47% at 1400 °C under inert atmosphere.

Finally, although the overall mechanical and metallurgical performance of such aggregates is comparable to or even better than that of pellets typically used in shaft furnaces (e.g., survival of 7 drops, CCS of 9.5 MPa, bulk density of 2 g/cm^3, swelling less than 20%), the presence of harmful elements (e.g., S, K, Zn, Na, and Pb) makes their introduction into cupola furnaces preferable to blast furnace [24, 65].

Supplementary Information The online version contains supplementary material available at https://doi.org/10.1007/s40831-024-00825-2.

Acknowledgements The authors are thankful to Prof. Gianmarco Griffni and Eng. Emanuela Bellinetto for the TG-DSC measurements on starch.

Author Contributions Gianluca Dall'Osto: visualization, writing original draft, review and editing, resources, data curation; Davide Mombelli: conceptualization, methodology, validation, visualization, writing original draft; Valentina Trombetta: formal analysis, investigation, data curation; Carlo Mapelli: supervision.

Funding Open access funding provided by Politecnico di Milano within the CRUI-CARE Agreement. Open access funding provided by Politecnico di Milano within the CRUI-CARE Agreement.

Data Availability All data generated or analyzed during this study are included in this published article and its electronic supplementary material.

Declarations

Conflict of interest On behalf of all authors, the corresponding author states that there is no conflict of interest.

References

1. Golnaraghi Ghomi A, Asasian-Kolur N, Sharifian S, Golnaraghi A (2020) Biosorpion for sustainable recovery of precious metals from wastewater. J Environ Chem Eng 8:103996. https://doi.org/10.1016/j.jece.2020.103996
2. Jadhav UU, Hocheng H (2012) A review of recovery of metals from industrial waste. J Achiev Mater Manuf Eng 54:159–167
3. Linsong W, Peng Z, Yu F et al (2020) Recovery of metals from jarosite of hydrometallurgical nickel production by thermal treatment and leaching. Hydrometallurgy 198:105493. https://doi.org/10.1016/j.hydromet.2020.105493
4. Dutrizac JE, Jambor JL (2000) Jarosites and their application in hydrometallurgy. Rev Mineral Geochem 40:405–452. https://doi.org/10.2138/rmg.2000.40.8
5. Monhemius AJ (2017) The iron elephant: a brief history of hydrometallurgist's struggles with element element no. 26. CIM J. https://doi.org/10.15834/cimj.2017.21
6. Seyer S, Chen TT, Dutrizac JE (2001) Jarofix: addressing iron disposal in the zinc industry. JOM 53:32–35. https://doi.org/10.1007/s11837-001-0010-2
7. Chen TT, Dutrizac JE (2013) A mineralogical study of jarofix products for the stabilization of jarosite residues for disposal. Lead-Zinc 2000. Wiley, Hoboken, pp 917–934
8. Dutrizac JE (1984) The behavior of impurities during Jarosite precipitation. Hydrometallurgical process fundamentals. Springer, Boston, pp 125–169
9. Kumar Singh V, Manna S, Kumar Biswas J, Pugazhendhi A (2023) Recovery of residual metals from jarosite waste using chemical and biochemical processes to achieve sustainability: a state-of-the-art review. J Environ Manage 343:118221. https://doi.org/10.1016/j.jenvman.2023.118221
10. Calla-Choque D, Nava-Alonso F, Fuentes-Aceituno JC (2016) Acid decomposition and thiourea leaching of silver from hazardous jarosite residues: effect of some cations on the stability of the thiourea system. J Hazard Mater 317:440–448. https://doi.org/10.1016/j.jhazmat.2016.05.085
11. Calla-Choque D, Lapidus GT (2020) Acid decomposition and silver leaching with thiourea and oxalate from an industrial jarosite sample. Hydrometallurgy 192:105289. https://doi.org/10.1016/j.hydromet.2020.105289
12. Ntumba Malenga E, Mulaba-Bafubiandi AF, Nheta W (2015) Alkaline leaching of nickel bearing ammonium jarosite precipitate using KOH, NaOH and NH4OH in the presence of EDTA and Na2S. Hydrometallurgy 155:69–78. https://doi.org/10.1016/j.hydromet.2015.04.004
13. De-la-Cruz-Moreno JE, Ceniceros-Gómez AE, Morton-Bermea O, Hernández-Álvarez E (2021) Recovery of indium from jarosite residues of zinc refinery by a hydrometallurgical process. Hydrometall 203:105697. https://doi.org/10.1016/j.hydromet.2021.105697
14. Reyes IA, Patiño F, Flores MU et al (2017) Dissolution rates of jarosite-type compounds in H2SO4 medium: a kinetic analysis and its importance on the recovery of metal values from hydrometallurgical wastes. Hydrometall 167:16–29. https://doi.org/10.1016/j.hydromet.2016.10.025
15. Salinas E, Roca A, Cruells M et al (2001) Characterization and alkaline decomposition–cyanidation kinetics of industrial ammonium jarosite in NaOH media. Hydrometallurgy 60:237–246. https://doi.org/10.1016/S0304-386X(01)00149-9
16. Roca A, Patiño F, Viñals J, Núñez C (1993) Alkaline decomposition-cyanidation kinetics of argentojarosite. Hydrometall 33:341–357. https://doi.org/10.1016/0304-386X(93)90071-K
17. Patiño F, Viñals J, Roca A, Núñez C (1994) Alkaline decomposition-cyanidation kinetics of argentian plumbojarosite. Hydrometall 34:279–291. https://doi.org/10.1016/0304-386X(94)90066-3
18. Zhu D, Yang C, Pan J et al (2018) New pyrometallurgical route for separation and recovery of Fe, Zn, In, Ga and S from jarosite residues. J Clean Prod 205:781–788. https://doi.org/10.1016/j.jclepro.2018.09.152
19. Mombelli D, Mapelli C, Barella S et al (2019) Jarosite wastes reduction through blast furnace sludges for cast iron production. J Environ Chem Eng. https://doi.org/10.1016/j.jece.2019.102966
20. Mombelli D, Mapelli C, Di Cecca C et al (2018) Characterization of cast iron and slag produced by jarosite sludges reduction via arc transferred plasma (ATP) reactor. J Environ Chem Eng 6:773–783. https://doi.org/10.1016/j.jece.2018.01.006
21. Sharma P (2016) Feasibility study of industrial jarosite waste as vital material for construction: positive and negative aspects. Malays J Civ Eng 28:139–154
22. Willms T, Echterhof T, Steinlechner S et al (2020) Investigation on the chemical and thermal behavior of recycling agglomerates from EAF by-products. Appl Sci (Switz) 10:1–14. https://doi.org/10.3390/app10228309
23. Echterhof T, Willms T, Preiß S et al (2019) Developing a new process to agglomerate secondary raw material fines for recycling

in the electric arc furnace - The fines2EAF project. Metall Italiana 111:31–40
24. Mombelli D, Dall'Osto G, Trombetta V, Mapelli C (2023) Comparison of the reduction behavior through blast furnace sludge of two industrial jarosites. J Environ Chem Eng 11:109360. https://doi.org/10.1016/j.jece.2023.109360
25. Mombelli D, Gonçalves DL, Mapelli C et al (2021) Processing and characterization of self-reducing briquettes made of Jarosite and blast furnace sludges. J Sustain Metall. https://doi.org/10.1007/s40831-021-00419-2
26. International Organization for Standardization (2017) Geotechnical investigation and testing—Identification and classification of soil—Part 1: Identification and description (ISO 14688-1:2017)
27. American Society for Testing and Materials International (2019) Standard guide for powder particle size analysis (ASTM E2651−19)
28. Abdelrahim A (2018) Recycling of steel plant by-products by cold bonded briquetting
29. International Organization for Standardization (2015) Iron ore pellets for blast furnace and direct reduction feedstocks—determination of the crushing strength (BS ISO 4700:2015)
30. American Society for Testing and Materials International (2019) Standard test method of drop shatter test for coal (ASTM D440-07)
31. International Organization for Standardization (2015) Iron ores for shaft direct-reduction feedstocks. Determination of the reducibility index, final degree of reduction and degree of metallization (BS ISO 11258:2015)
32. Montgomery DC (2012) Design and analysis of experiments, 8th edn. Wiley, New York
33. (2004) Undesired agglomeration: methods of avoiding or lessening its effect. In: Agglomeration set. Wiley. pp 23–36
34. Pham AM, Descantes Y, de Larrard F (2011) Determination of sieve grading curves using an optical device. Mechatron 21:298–309. https://doi.org/10.1016/j.mechatronics.2010.11.008
35. Bartley PC, Jackson BE, Fonteno WC (2019) Effect of particle length to width ratio on sieving accuracy and precision. Powder Technol 355:349–354. https://doi.org/10.1016/j.powtec.2019.07.016
36. Sanna AL, Pia G, Delogu F (2023) kinetics of grain size reduction in minerals undergoing ball milling. Trans Indian Inst Met. https://doi.org/10.1007/s12666-023-03034-9
37. Li Z, Zou H (2022) Optimization of biomass fuel cold briquetting parameters based on response surface analysis. J Inst Eng (India) Ser C 103:459–472. https://doi.org/10.1007/s40032-021-00782-9
38. Rodriguez-Navarro C, Doehne E, Sebastian E (2000) How does sodium sulfate crystallize? Implications for the decay and testing of building materials. Cem Concr Res 30:1527–1534. https://doi.org/10.1016/S0008-8846(00)00381-1
39. Saidov TA, Pel L, Kopinga K (2015) Crystallization pressure of sodium sulfate heptahydrate. Cryst Growth Des 15:2087–2093. https://doi.org/10.1021/cg501537h
40. Yu S, Oguchi CT (2013) Is sheer thenardite attack impotent compared with cyclic conversion of thenardite–mirabilite mechanism in laboratory simulation tests? Eng Geol 152:148–154. https://doi.org/10.1016/j.enggeo.2012.10.009
41. Germinario L, Oguchi CT (2022) Gypsum, mirabilite, and thenardite efflorescences of tuff stone in the underground environment. Environ Earth Sci 81:242. https://doi.org/10.1007/s12665-022-10344-6
42. Hoover R, Li YX, Hynes G, Senanayake N (1997) Physicochemical characterization of mung bean starch. Food Hydrocoll 11:401–408. https://doi.org/10.1016/S0268-005X(97)80037-9
43. Harun NY, Afzal MT (2016) Effect of particle size on mechanical properties of pellets made from biomass blends. Procedia Eng 148:93–99. https://doi.org/10.1016/j.proeng.2016.06.445
44. Mani S, Tabil LG, Sokhansanj S (2006) Effects of compressive force, particle size and moisture content on mechanical properties of biomass pellets from grasses. Biomass Bioenergy 30:648–654. https://doi.org/10.1016/j.biombioe.2005.01.004
45. Pang L, Yang Y, Wu L et al (2019) Effect of particle sizes on the physical and mechanical properties of briquettes. Energ (Basel) 12:3618. https://doi.org/10.3390/en12193618
46. Li Y, Chen H, Hammam A et al (2021) Study of an organic binder of cold-bonded briquettes with two different iron bearing materials. Mater 14:2952. https://doi.org/10.3390/ma14112952
47. Sen R, Wiwatpanyaporn S, Annachhatre AP (2016) Influence of binders on physical properties of fuel briquettes produced from cassava rhizome waste. Int J Environ Waste Manag 17:158. https://doi.org/10.1504/IJEWM.2016.076750
48. Anameric B, Kawatra SK (2007) Properties and features of direct reduced iron. Min Process Extr Metall Rev 28:59–116. https://doi.org/10.1080/08827500600835576
49. Ríos A, González M, Montes C et al (2020) Assessing the effect of fly ash with a high SO3 content in hybrid alkaline fly ash pastes (HAFAPs). Constr Build Mater 238:117776. https://doi.org/10.1016/j.conbuildmat.2019.117776
50. Tammann G, Oelsen W (1930) Die Reaktionen beim Zusammenschmelzen von Glassätzen. Z Anorg Allg Chem 193:245–269. https://doi.org/10.1002/zaac.19301930122
51. Samadhi TW, Jones LE, Clare AG (2003) Influence of carbon on SO_x emissions from glass processing. J Am Ceram Soc 86:2044–2049. https://doi.org/10.1111/j.1151-2916.2003.tb03606.x
52. Weast RC (1986) CRC handbook of chemistry and physics
53. Iljana M, Mattila O, Alatarvas T et al (2012) Dynamic and isothermal reduction swelling behaviour of olivine and acid iron ore pellets under simulated blast furnace shaft conditions. ISIJ Int 52:1257–1265. https://doi.org/10.2355/isijinternational.52.1257
54. Reddy DS, Chang H-H, Tsai M-Y et al (2023) Swelling and softening behavior of iron ore-spent mushroom substrate composite pellets during carbothermal reduction. J Market Res 22:1999–2007. https://doi.org/10.1016/j.jmrt.2022.12.022
55. Huang T-Y, Maruoka D, Murakami T, Kasai E (2019) Morphology change and carburization characteristic of iron ore-coal composite during reduction under a simulated condition of blast furnace. ISIJ Int 59:1982–1990. https://doi.org/10.2355/isijinternational.ISIJINT-2019-178
56. Murakami T, Takahashi T, Fuji S et al (2017) Development of manufacturing principle of porous iron by carbothermic reduction of composite of hematite and biomass char. Mater Trans 58:1742–1748. https://doi.org/10.2320/matertrans.M2017232
57. Singh M, Björkman B (2004) Effect of reduction conditions on the swelling behaviour of cement-bonded briquettes. ISIJ Int 44:294–303. https://doi.org/10.2355/isijinternational.44.294
58. Han H, Duan D, Yuan P (2014) Binders and bonding mechanism for RHF briquette made from blast furnace dust. ISIJ Int 54:1781–1789. https://doi.org/10.2355/isijinternational.54.1781
59. Lund D, Lorenz KJ (1984) Influence of time, temperature, moisture, ingredients, and processing conditions on starch gelatinization. C R C Critical Rev Food Sci Nutr 20:249–273. https://doi.org/10.1080/10408398409527391
60. Sandhu K, Singh N (2007) Some properties of corn starches II: physicochemical, gelatinization, retrogradation, pasting and gel textural properties. Food Chem 101:1499–1507. https://doi.org/10.1016/j.foodchem.2006.01.060
61. Yan W, Yin L, Zhang M et al (2021) Gelatinization, retrogradation and gel properties of wheat starch-wheat bran arabinoxylan complexes. Gels 7:200. https://doi.org/10.3390/gels7040200
62. Anameric B, Rundman KB, Kawatra SK (2006) Carburization effects on pig iron nugget making. Min Metall Explor 23:139–150. https://doi.org/10.1007/BF03403201

63. Han J, Liu W, Zhang T et al (2017) Mechanism study on the sulfidation of ZnO with sulfur and iron oxide at high temperature. Sci Rep 7:42536. https://doi.org/10.1038/srep42536
64. Ghosh A, Chatterjee A (2008) Ironmaking and steelmaking theory and practice. New Delhi
65. Seetharaman S (2013) Treatise on process metallurgy. Industrial processes, vol 3. Newnes, Oxford

Authors and Affiliations

G. Dall'Osto[1] · D. Mombelli[1] · V. Trombetta[1] · C. Mapelli[1]

✉ D. Mombelli
davide.mombelli@polimi.it

[1] Dipartimento di Meccanica, Politecnico di Milano, Via la Masa 1, 20156 Milan, Italy